AFRL-RV-PS-
TP-2012-0026

MAGNETIC FIELD-LINE LENGTHS IN INTERPLANETARY CORONAL MASS EJECTIONS INFERRED FROM ENERGETIC ELECTRON EVENTS (POSTPRINT)

S.W. Kahler, et al.

03 May 2012

Technical Paper

AIR FORCE RESEARCH LABORATORY
Space Vehicles Directorate
3550 Aberdeen Ave SE
AIR FORCE MATERIEL COMMAND
KIRTLAND AIR FORCE BASE, NM 87117-5776

REPORT DOCUMENTATION PAGE

Form Approved
OMB No. 0704-0188

1. REPORT DATE *(DD-MM-YYYY)*	**2. REPORT TYPE**	**3. DATES COVERED** *(From - To)*
03-05-2012	Technical Paper	1 Oct 2007 – 13 Jul 2011

4. TITLE AND SUBTITLE
Magnetic Field-Line Lengths in Interplanetary Coronal Mass Ejections Inferred From Energetic Electron Events (Postprint)

5a. CONTRACT NUMBER
In-House

5b. GRANT NUMBER

5c. PROGRAM ELEMENT NUMBER
62601F

6. AUTHOR(S)
S.W. Kahler, D.K. Haggerty, and I.G. Richardson

5d. PROJECT NUMBER
1010

5e. TASK NUMBER
PPM00004579

5f. WORK UNIT NUMBER
EF004380

7. PERFORMING ORGANIZATION NAME(S) AND ADDRESS(ES)

Air Force Research Laboratory
Space Vehicles Directorate
3550 Aberdeen Ave SE
Kirtland AFB, NM 87117-5776

8. PERFORMING ORGANIZATION REPORT NUMBER

AFRL-RV-PS-TP-2012-0026

9. SPONSORING / MONITORING AGENCY NAME(S) AND ADDRESS(ES)

10. SPONSOR/MONITOR'S ACRONYM(S)
AFRL/RVBXS

11. SPONSOR/MONITOR'S REPORT NUMBER(S)

12. DISTRIBUTION / AVAILABILITY STATEMENT

Approved for public release; distribution is unlimited. (66ABW-2010-1529, dtd 21 Dec 2010)

13. SUPPLEMENTARY NOTES
The Astrophysical Journal, 736:106 (9pp); doi: 10.1088/0004-637X/736/2/106; Government purpose rights.

14. ABSTRACT
About one quarter of the observed interplanetary coronal mass ejections (ICMEs) are characterized by enhanced magnetic fields that smoothly rotate in direction over timescales of about 10–50 hr. These ICMEs have the appearance of magnetic flux ropes and are known as "magnetic clouds" (MCs). The total lengths of MC field lines can be determined using solar energetic particles of known speeds when the solar release times and the 1 AU onset times of the particles are known. A recent examination of about 30 near-relativistic (NR) electron events in and near 8 MCs showed no obvious indication that the field-line lengths were longest near the MC boundaries and shortest at the MC axes or outside the MCs, contrary to the expectations for a flux rope. Here we use the impulsive beamed NR electron events observed with the Electron Proton and Alpha Monitor instrument on the *Advanced Composition Explorer* spacecraft and type III radio bursts observed on the *Wind* spacecraft to determine the field-line lengths inside ICMEs included in the catalog of Richardson & Cane. In particular, we extend this technique to ICMEs that are not MCs and compare the field-line lengths inside MCs and non-MC ICMEs with those in the ambient solar wind outside the ICMEs. No significant differences of field-line lengths are found among MCs, ICMEs, and the ambient solar wind. The estimated number of ICME field-line turns is generally smaller than those deduced for flux-rope model fits to MCs. We also find cases in which the electron injections occur in solar active regions (ARs) distant from the source ARs of the ICMEs, supporting CME models that require extensive coronal magnetic reconnection with surrounding fields. The field-line lengths are found to be statistically longer for the NR electron events classified as ramps and interpreted as shock injections somewhat delayed from the type III bursts. The path lengths of the remaining spike and pulse electron events are compared with model calculations of solar wind field-line lengths resulting from turbulence and found to be in good agreement.

15. SUBJECT TERMS
Acceleration of particles, interplanetary medium, Sun: coronal mass ejections (CMEs), Sun: particle emission

16. SECURITY CLASSIFICATION OF:			**17. LIMITATION OF ABSTRACT**	**18. NUMBER OF PAGES**	**19a. NAME OF RESPONSIBLE PERSON**
a. REPORT	**b. ABSTRACT**	**c. THIS PAGE**			Donald Norquist
Unclassified	Unclassified	Unclassified	Unlimited	12	**19b. TELEPHONE NUMBER** *(include area code)*

The Astrophysical Journal, 736:106 (9pp), 2011 August 1 doi:10.1088/0004-637X/736/2/106

MAGNETIC FIELD-LINE LENGTHS IN INTERPLANETARY CORONAL MASS EJECTIONS INFERRED FROM ENERGETIC ELECTRON EVENTS

S. W. Kahler[1], D. K. Haggerty[2], and I. G. Richardson[3,4]
[1] Air Force Research Laboratory, RVBXS, 29 Randolph Rd, Hanscom AFB, MA 01731, USA; AFRL.RVB.PA@hanscom.af.mil
[2] The Johns Hopkins University, Applied Physics Laboratory, 11100 Johns Hopkins Road, Laurel, MD 20723, USA
[3] Code 661, NASA Goddard Space Flight Center, Greenbelt, MD 20771, USA
Received 2011 January 19; accepted 2011 May 12; published 2011 July 13

ABSTRACT

About one quarter of the observed interplanetary coronal mass ejections (ICMEs) are characterized by enhanced magnetic fields that smoothly rotate in direction over timescales of about 10–50 hr. These ICMEs have the appearance of magnetic flux ropes and are known as "magnetic clouds" (MCs). The total lengths of MC field lines can be determined using solar energetic particles of known speeds when the solar release times and the 1 AU onset times of the particles are known. A recent examination of about 30 near-relativistic (NR) electron events in and near 8 MCs showed no obvious indication that the field-line lengths were longest near the MC boundaries and shortest at the MC axes or outside the MCs, contrary to the expectations for a flux rope. Here we use the impulsive beamed NR electron events observed with the Electron Proton and Alpha Monitor instrument on the *Advanced Composition Explorer* spacecraft and type III radio bursts observed on the *Wind* spacecraft to determine the field-line lengths inside ICMEs included in the catalog of Richardson & Cane. In particular, we extend this technique to ICMEs that are not MCs and compare the field-line lengths inside MCs and non-MC ICMEs with those in the ambient solar wind outside the ICMEs. No significant differences of field-line lengths are found among MCs, ICMEs, and the ambient solar wind. The estimated number of ICME field-line turns is generally smaller than those deduced for flux-rope model fits to MCs. We also find cases in which the electron injections occur in solar active regions (ARs) distant from the source ARs of the ICMEs, supporting CME models that require extensive coronal magnetic reconnection with surrounding fields. The field-line lengths are found to be statistically longer for the NR electron events classified as ramps and interpreted as shock injections somewhat delayed from the type III bursts. The path lengths of the remaining spike and pulse electron events are compared with model calculations of solar wind field-line lengths resulting from turbulence and found to be in good agreement.

Key words: acceleration of particles – interplanetary medium – Sun: coronal mass ejections (CMEs) – Sun: particle emission

Online-only material: color figure

1. INTRODUCTION

1.1. ICMEs and Magnetic Flux Ropes

Coronal mass ejections (CMEs) are the most energetic of solar transient events and merit continued observation and study because of their impact as drivers of space weather. When CMEs appear near solar central meridian, they are usually detected within several days as interplanetary CMEs (ICMEs) at 1 AU that may be identified based on a number of characteristic particle and magnetic field signatures (Zurbuchen & Richardson 2006, and references therein). About one quarter of the ICMEs, termed "magnetic clouds" (MCs) (Klein & Burlaga 1982), show a characteristic signature of a smoothly rotating, enhanced low-β magnetic field (Cane & Richardson 2003). MCs have been extensively modeled as magnetic flux ropes, beginning with a locally symmetric force-free field approximation fitted by a Lundquist solution that yields a toroidal solution with field lines of increasing pitch angle, or twist, from the MC axis to the boundary (e.g., Lepping et al. 1990). Recent modeling has used more complex assumptions about flux-rope geometries and plasma pressure to fit in situ MC observations from multiple spacecraft (Liu et al. 2008a, 2008b; Nakagawa & Matsuoka 2010) and appears to confirm the basic assumed structure.

CME structures resembling flux ropes are often seen in coronagraph observations (e.g., Wang & Sheeley 2006), and recent detailed studies of CME trajectories and associated flare timescales have provided support for an erupting flux-rope model (Temmer et al. 2010; Chen & Kunkel 2010). Recent complementary studies of *STEREO* coronagraph observations of prominent CMEs and their counterpart ICMEs at 1 AU provide strong confirmation of the fundamental CME/ICME flux-rope structure (Liu et al. 2008a, 2008b; Kilpua et al. 2009; Davis et al. 2009; Möstl et al. 2009a, 2009b; Wood & Howard 2009; Lynch et al. 2010; Wood et al. 2010; Byrne et al. 2010; Kunkel & Chen 2010).

When a preceding CME can be associated with an MC, the MC magnetic flux inferred from a model fit may be compared with the magnetic flux of the CME solar source region. Leamon et al. (2004) found the MC magnetic flux to be comparable to and proportional to that of the associated active region (AR) for 12 MCs. However, the total field twists of the MCs were about an order of magnitude greater than those of the ARs. Qiu et al. (2007) did a more direct comparison of the magnetic fluxes of nine modeled MCs with the total reconnection fluxes measured in their associated solar flare ribbons. They found the MC poloidal flux to be comparable to the flare reconnection flux and the toroidal (axial) MC flux to be a fraction of the reconnection flux. The further finding that the magnetic flux of the solar dimming region is comparable to the MC toroidal flux

[4] CRESST and Department of Astronomy, University of Maryland, College Park, MD 20742, USA.

satisfies the idea that the dimming regions are the footpoints of the flux ropes forming the MCs. These MC models and solar observations provide a compelling view of the origin and transport of magnetic flux from solar eruptive events to 1 AU, at least for the MCs.

Nevertheless, several basic questions about ICMEs remain open. Pitch-angle distributions of solar wind heat-flux electrons indicate that some regions within MCs maintain magnetic connectivity back to the corona at both footpoints of the flux rope, but the detailed MC field-line coronal connections and their evolution in time remain unclear (Attrill et al. 2008). A fundamental question is why MC flux-rope structures are found in only one quarter of all ICMEs (Moldwin et al. 2009) if indeed all CMEs originate as flux ropes at the Sun (Krall 2007). The small fraction of MCs detected in ICMEs might be partially due to a selection effect against MC encounters at large closest approach distances, i.e., the closest distance between the observer and the cloud's axis (Lepping & Wu 2010).

The questions of ICME structure and coronal connectivity are matters of magnetic field geometry and topology, respectively, that are difficult to address observationally even with the combined solar/interplanetary imaging and in situ field measurements at 1 AU discussed above (Jacobs et al. 2009). One possibility for probing remote ICME field geometry is by observing the Faraday rotation (FR) of microwave emission from sources occulted by an ICME. Recent MC modeling of several FR structures observed with carrier signals from the *Pioneer* and *Helios* spacecraft (Liu et al. 2007; Jensen & Russell 2008) suggests that a sky mapping of FR from galactic sources could provide important details of ICME magnetic structures. The FR technique has significant limitations, however, as discussed by Broderick & Blandford (2010).

1.2. Energetic Particle Events as Probes of ICME Topology

Energetic particles, in particular, fast ($v \geqslant 0.1$ AU hr^{-1}) electrons, have thus far proved to be the best means of probing the magnetic structures of MCs because their small gyroradii ($\leqslant 10^2$ km in a 10 nT field) confine them to propagate closely following the field lines. Solar wind heat-flux electrons have been widely used as a tool to probe magnetic structures of the solar wind (e.g., Crooker & Pagel 2008) and of MCs (Crooker et al. 2008). In a pioneering work, Larson et al. (1997) used $E \sim 200$ eV heat-flux electron pitch-angle distributions and $E \geqslant 30$ keV solar-electron event onsets observed inside an MC on 1995 October 18 and 19 to set limits on the solar magnetic connection and field-line lengths, respectively. Inferred field-line lengths provide a fundamental test of MC flux-rope models, and the 3 AU length found for a solar-electron event detected near the boundary of the 1995 October MC provided strong support for such models. However, that observation remained the unique event available for comparison with various MC flux-rope models (Leamon et al. 2004; Dasso et al. 2006; Qiu et al. 2007; Yamamoto et al. 2010) until Kahler et al. (2011) applied the method to eight MCs by using $E \geqslant 30$ keV electron observations from the 3DP instrument on the *Wind* spacecraft. They found poor correlations between the inferred electron path lengths Le and the field-line lengths calculated for two MC models. The only electron path length $Le > 3.2$ AU in their survey was the same as that found with the same 3DP electron data by Larson et al. (1997) for the 1995 October MC. The electron path lengths of that event matched well their model MC field-line lengths. However, the MC model path lengths away from the MC boundaries are generally only slightly longer than an assumed spiral field-line length of 1.2 AU and hence not a good test of the models. The model tests must be done in the peripheral regions near the MC boundaries (Kahler et al. 2011), where the field-line twists and lengths are greatest.

In this work, we check and extend the result of Kahler et al. (2011) by analyzing another set of $E > 30$ keV solar-electron path lengths, this time in ICMEs not all of which are MCs. The data selection and analysis are described in Section 2. The distributions of the calculated near-relativistic (NR) electron path lengths Le within and outside ICMEs are presented in Sections 3.1 and 3.2. In Section 3.3, we compare values of Le with their electron event types and with calculated turbulent field-line lengthening. To look for restructuring of the ICME field lines, the solar sources of the NR electron events are compared with the sources of their ICMEs in Section 3.4. The implications of the results for ICME field-line lengths and coronal restructuring are discussed in Section 4 and summarized in Section 5.

2. DATA ANALYSIS

2.1. EPAM Beamed Electron Events

The basic data set used here is the list of beamed $E > 38$ keV electron events observed with the Electron Proton and Alpha Monitor (EPAM) on the *Advanced Composition Explorer* (*ACE*) spacecraft. That instrument observes electrons in four energy channels spanning the nominal energy range 38 keV $< E <$ 315 keV with three detector telescopes (Gold et al. 1998). Of the observed solar-electron events about one-third with unambiguous onsets, velocity dispersion, and field-aligned (beam-like) angular distributions (Haggerty & Roelof 2002; Haggerty et al. 2003) are selected for analysis. The onset time of each event is when the electron intensity is first observed rising above the pre-event intensity of the highest observed energy channel (Haggerty & Roelof 2002), which is not affected by electron scattering in the detector (Haggerty & Roelof 2006a). This criterion excludes events observed only in the lowest energy channel. A cumulative timing error of $\sim$1 minute year^{-1} in the EPAM data has been corrected (Simnett 2007). Here we use the subset of 204 beamed electron events observed from launch in 1997 through the end of 2005 (Haggerty & Roelof 2009).

Nearly every beamed electron event is temporally associated with a decametric (2–14 MHz) type III radio burst observed with the WAVES detector (Bougeret et al. 1995) on the *Wind* spacecraft. Only 8 of the 204 events had no associated type III burst at either 2 or 14 MHz, and one was observed at only 2 MHz, leaving 195 events for analysis. Since the nominal 1.2 AU electron travel times range only from $\sim$21 to 14 minutes for the mean energies of the second to the fourth EPAM energy channels, the type III burst association is rarely ambiguous, as shown in Figure 1 for two events. The timing fiducials for each event are the onset of the 14 MHz type III burst and the electron onset of the highest observed EPAM energy channel.

2.2. Basic Assumptions of Electron Transport

When the energetic electrons are assumed to travel a nominal distance of 1.2 AU scatter free along the Parker spiral magnetic field lines, the solar injection times can be deduced. Considerable work has been done to compare the EPAM electron onset times with the times of solar flares and CMEs to understand the conditions of electron acceleration and injection. A consistent result, observed with both the EPAM (e.g., Maia & Pick 2004;

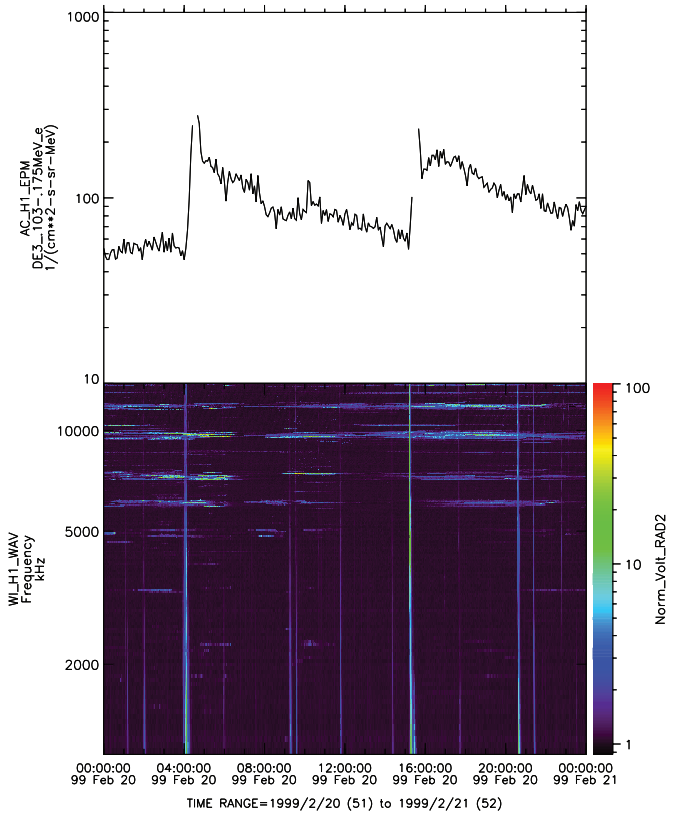

Figure 1. Top: plot of the EPAM DE3 (103 keV $< E <$ 175 keV) electron intensities on 1999 February 20 showing two events that occurred in a single MC. Bottom: spectrogram of the WAVES/*Wind* associated 1–14 MHz emission. The EPAM electron events of the study are almost always unambiguously associated with a WAVES type III burst, which we use as the fiducial for the time of initial electron injection.

(A color version of this figure is available in the online journal.)

Haggerty & Roelof 2009) and the 3DP detector on *Wind* (Klein et al. 2005), has been that while in some events $E > 40$ keV electron injections occur simultaneously with metric/decametric type III bursts, most inferred injections are delayed by up to ~30 minutes from the type III bursts (Nindos et al. 2008). Furthermore, with 3DP observations Klein et al. (2005) found that 30 of 40 delayed injections were accompanied by metric radio bursts. However, Kahler et al. (2007) found no single radio signature to be characteristic of the inferred electron injection times of 80 3DP electron events. Two possible interpretations of the delayed injections are that the electrons are accelerated after the type III bursts in CME-driven shocks (Simnett et al. 2002) or in coronal magnetic reconnection regions (Maia & Pick 2004; Klein et al. 2005). To complete the picture, it is further assumed that electrons injected in the type III bursts are usually confined to $E \leqslant 10$ keV (Wang et al. 2006; Haggerty & Roelof 2006b) and that type III bursts do not accompany the delayed $E > 40$ keV electron injections. An alternative interpretation of the delayed injections is that all the electrons are initially injected during the accompanying type III bursts, but the 1 AU arrival times are delayed due to interplanetary scattering (Cane 2003). Another alternative is that the assumption of a 1.2 AU travel distance is invalid because solar wind turbulence extends the field-line lengths by factors of ~1.3–1.6 (Ragot 2006; Ragot & Kahler 2008; Kahler et al. 2011).

In this analysis, we assume that the initial solar injections of the $E > 40$ keV electrons coincide with the decametric type III

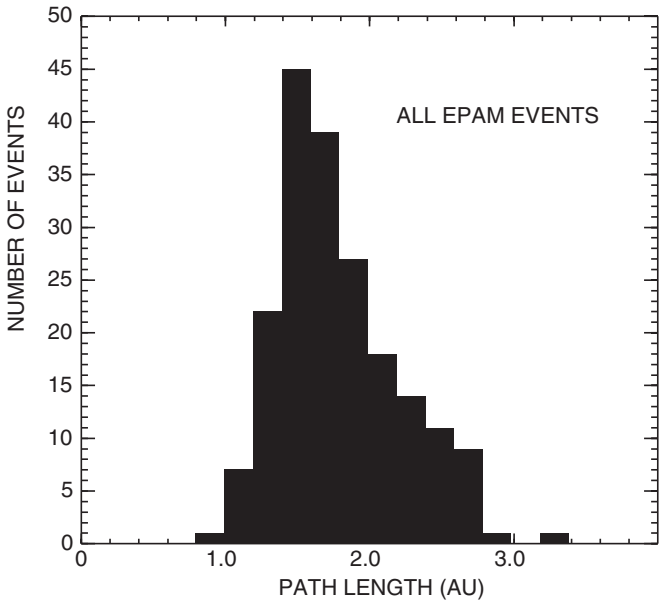

Figure 2. Plot of the *Le* distribution for all 195 EPAM NR electron events.

burst onsets and that the propagation times to 1 AU are due to scatter-free electron propagation along variable field-line path lengths. From the known speeds of the first arriving beamed electrons we can deduce the total lengths of the field lines followed by the electrons, as was done by Larson et al. (1997) and Kahler et al. (2011). This is a reversal of the assumption in the earlier cited studies that the path length was known (1.2 AU) and that the electron speed could be used to deduce the event injection time. If the injections are in fact delayed beyond the type III burst times, then our technique returns upper bounds on the electron path lengths, which, because of the small electron gyroradii ($\leqslant$100 km in a 10 nT field), are equivalent to the field-line lengths. We use the technique to determine the lengths of field lines in and around ICMEs, some of which may be considerably longer than 1.2 AU (Kahler et al. 2011). The terms electron path lengths (*Le*) and field-line lengths will hereafter be used interchangeably.

3. RESULTS

3.1. The Calculated Electron Path Lengths Le Inside and in the Vicinity of ICMEs

For all 195 electron events, we calculated the electron path lengths *Le* for the first arriving electrons assuming (1) solar injections 8.33 minutes before the observed 14 MHz type III burst onsets and (2) 1 AU electron travel speeds corresponding to the mean energy of the highest observed EPAM energy channel (0.0585 AU minute^{-1} for channel 2, 0.0734 AU minute^{-1} for channel 3, and 0.0876 AU minute^{-1} for channel 4). Figure 2 shows a plot of all 195 *Le* values. The mean and median *Le* are 1.79 and 1.69 AU, respectively, for all events; $Le > 2.7$ AU for only four events. The sample number, mean value, standard deviation, and median value of each *Le* distribution group are given in Table 2.

We compared the 195 EPAM electron onsets with the times of near-Earth ICMEs in the catalog of Richardson & Cane (2010), which were selected on the basis of solar wind composition and charge states as well as other solar wind plasma and magnetic field parameters. Each ICME was assigned to one of the following three classes based on how closely its magnetic

Table 1
EPAM NR Electron Events in the Vicinity of ICMEs

Date[a]	Electron Onset[b]	14 MHz Onset[b]	ICME Type[c]	Normal[d] Position	*Le* (AU)
1997 Nov 23	10.32	10.01	2	0.82	1.56
1998 May 6	08.14	08.03	0	0.54	1.32
1998 Jul 11∗	13.00	12.78	0	0.21	1.88
1998 Jul 12∗	01.64	01.46	0	0.40	1.43
1998 Aug 13	18.08	17.91	1	1.11	1.63
1998 Sep 25∗	22.60	22.26	2	0.49	2.10
1998 Sep 26∗	16.56	16.39	2	1.01	1.37
1998 Sep 26∗	18.36	18.18	2	1.07	1.44
1998 Sep 27∗	1.21	0.88	2	1.26	1.63
1999 Feb 16	3.46	3.29	1	−0.58	1.34
1999 Feb 20∗	04.20	04.08	2	0.76	1.16
1999 Feb 20∗	15.35	15.21	2	0.97	1.43
1999 Mar 10	23.19	22.77	0	0.18	1.98
1999 Apr 22	10.01	09.67	2	0.88	2.11
1999 Jun 4	7.31	7.14	1	1.41	1.65
1999 Jun 29	12.83	12.66	0	1.30	1.38
2000 Jan 22	19.36	19.11	1	0.28	1.69
2000 Mar 2	8.72	8.41	0	1.25	2.37
2000 Mar 18	21.17	20.94	0	−0.50	1.94
2000 Jun 10	17.15	17.17	0	1.00	1.82
2000 Jul 12	20.32	20.21	2	0.78	1.35
2000 Oct 30	3.27	2.90	2	1.22	2.67
2001 Apr 2	22.01	21.81	1	0.71	1.75
2001 Apr 14	17.60	17.50	0	1.20	1.26
2001 Apr 30	11.13	10.97	2	0.75	1.58
2001 May 31	09.19	09.06	2	0.94	1.40
2001 Sep 24	10.87	10.59	1	0.50	2.21
2002 Mar 22	11.29	10.90	0	1.34	2.32
2002 Apr 11	16.51	16.31	1	−0.24	1.80
2002 Apr 21	01.56	01.34	2	0.61	1.92
2002 Aug 4	7.61	7.29	2	1.17	2.42
2002 Aug 19∗	21.21	21.02	1	0.18	1.73
2002 Aug 20∗	01.88	01.65	1	0.28	1.90
2002 Aug 20∗	08.65	08.43	1	0.41	1.89
2003 May 31	02.63	02.37	0	0.17	2.08
2003 Oct 28	11.29	11.11	0	1.38	1.68
2004 Sep 19	17.46	17.34	1	0.82	1.40
2005 Jan 20	6.85	6.75	0	1.14	1.24
2005 May 16	02.74	02.67	2	0.23	1.12
2005 Jun 12	16.35	15.95	2	0.07	1.91

Notes.
[a] "∗" indicates multiple events in the same ICMEs.
[b] In decimal hours UT.
[c] 0: no MC-like magnetic field features; 1: evidence of a rotation in the magnetic field direction, but overall magnetic field characteristics do not meet those of an MC; 2: includes an MC.
[d] Normalized position relative to ICME interval. Position <0 precedes the ICME; position >1 follows the ICME.

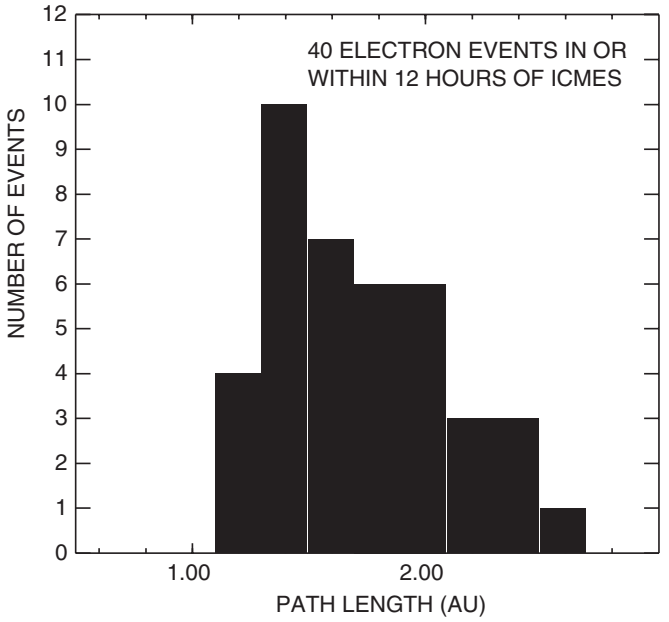

Figure 3. Plot of *Le* for 24 EPAM NR electron events inside ICMEs and 16 events within 12 hr of ICME boundaries. The 40 events are a subset of the 195 events of Figure 2.

Table 2
Field-line Lengths *Le* for Different Electron Event Classes

Electron Event Class	Number Events	Mean *Le* (AU)	Median *Le* (AU)
All events	195	1.79 ± 0.42	1.69
Non-ICMEs	155	1.80 ± 0.43	1.70
All ICMEs	40	1.72 ± 0.37	1.68
ICME class 0	13	1.75 ± 0.39	1.82
ICME class 1	11	1.73 ± 0.24	1.73
ICME class 2	16	1.70 ± 0.45	1.57
Inside ICMEs	24	1.70 ± 0.32	1.74
Outside ICMEs	16	1.76 ± 0.46	1.64
Spikes (S)	47	1.61 ± 0.34	1.52
Pulses (P)	53	1.66 ± 0.28	1.63
Combined S/P	100	1.64 ± 0.31	1.59
Ramps	95	1.94 ± 0.47	1.90
3DP MCs	30	2.28 ± 0.79	2.00

structure matched the classical MC definition (Klein & Burlaga 1982): class 0, no magnetic features of an MC; class 1, evidence of a rotation in the magnetic field direction, but overall no magnetic signature of an MC; and class 2, including an MC. The boundaries of ICMEs of class 2 often extended beyond the included MCs, so the MC intervals were also noted. We found 6 EPAM events in class 0 ICMEs (no MC-like fields), 7 in class 1 (evidence of a field rotation), and 11 in class 2 (containing an MC). Those 24 EPAM events are listed in Table 1. The first four table columns give the event date, electron onset time, 14 MHz onset time, and ICME type. The last column gives the inferred path length *Le*. In three cases multiple EPAM events occurred in the same ICME, so the total number of different ICMEs is 20. The fraction of electron events occurring inside ICME intervals is 24/204 = 0.118, very close to the 0.114 fraction of the total 1997–2005 era consisting of the ICME periods and consistent with a random distribution of electron events with respect to the ICME periods.

Magnetic field lines surrounding an ICME may have been extended by draping (McComas et al. 1989; Odstrcil & Pizzo 1999; Jones et al. 2002; Owens & Cargill 2004), so we also included all electron events with onsets ⩽12 hr from an ICME boundary, which added another 16 events to Table 1. A histogram of the combined 40 *Le* values obtained within and near ICMEs is shown in Figure 3. The mean (median) value of *Le* is 1.72 (1.68) AU for the ICME events. The mean (median) is 1.80 (1.70) AU for the distribution of the 155 non-ICME events shown in Figure 4. The non-ICME event standard deviation of 0.43 AU is only slightly larger than the 0.37 AU value of the 40 ICMEs. The *Le* distributions of Figures 3 and 4 therefore show no significant differences.

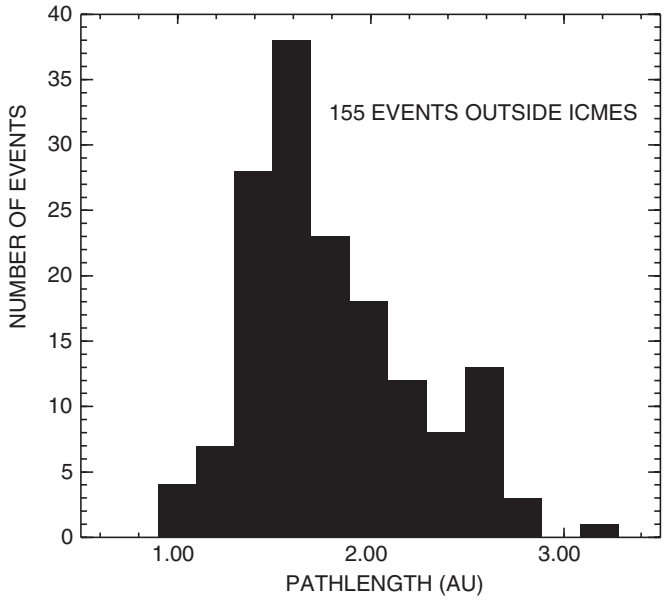

Figure 4. Distribution of *Le* for the 155 EPAM NR electron events ⩾12 hr outside the ICMEs.

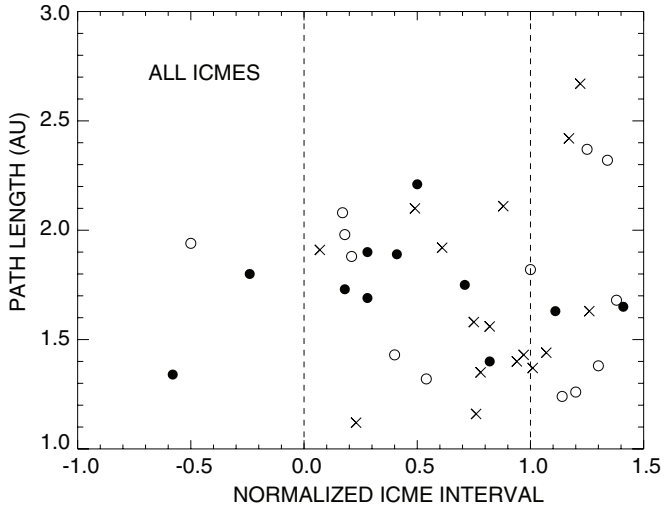

Figure 5. Superposed epoch plot of *Le* for all ICMEs, combining 16 EPAM NR electron events ⩽12 hr from ICME boundaries (vertical dashed lines) and the 24 events inside the boundaries. Open circles, solid circles, and crosses are class 0, 1, and 2 ICMEs, respectively.

3.2. Superposed Epoch Analysis of Electron Path Lengths Le in the Vicinity of ICMEs

For each event of Table 1 we calculated the electron onset time relative to a normalized unit ICME interval based on the ICME boundaries of Richardson & Cane (2010). The fifth column of Table 1 gives the normalized times, for which the electron events preceding or following the ICME intervals are indicated with values <0 and >1.0, respectively. The superposed epoch plot of the 40 ICME *Le* values is presented in Figure 5. Events within the three classes of ICMEs are denoted separately and the 16 additional electron events outside the ICME interval are also included. The mean and median *Le* for each ICME class is: class 0, 1.75 and 1.82 AU; class 1, 1.73 and 1.73 AU; and class 2, 1.70 and 1.57 AU. Thus, we find no obvious difference among the three classes or between the 16 events outside the ICME boundaries and the 24 events inside. There is also no tendency for a systematic variation of *Le* with time from the ICME boundaries.

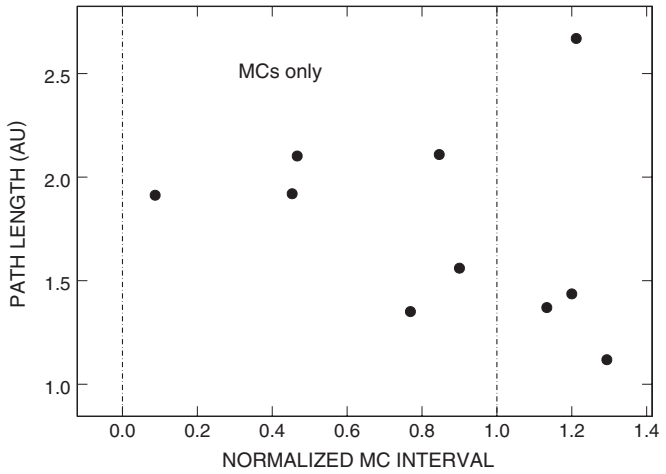

Figure 6. Superposed epoch plot of *Le* for all class 2 ICMEs, the MCs, normalized to the MC boundaries (vertical dashed lines) and including only EPAM NR electron events within a range of 40% of their MC intervals.

To compare our results with those of the MCs of Kahler et al. (2011), we have calculated the event times of the 16 class 2 ICMEs (Table 1 and Figure 5) normalized to the boundaries of the MCs, which may lie within the ICME intervals. The 10 events occurring within the normalized MC time intervals of −0.6 to 1.4 are shown in Figure 6. There are only six electron events inside and four outside the normalized MC boundaries, but again the boundaries do not order the values of *Le*. In general, we find no distinction of *Le* between ICMEs of any class and non-ICMEs.

3.3. Electron Event Types and Le

Haggerty & Roelof (2009) have classified the EPAM NR electron events in three categories defined by their intensity–time decay profiles: spikes, pulses, and ramps. They concluded that events in the first two categories are due to low-coronal explosive events while ramps are associated with injections from CME-driven shocks. This implies that our assumption of injections coincident with decametric type III bursts is correct for the spikes and pulses but is likely to imply an injection that is too early for most ramps, which are due to delayed injections from shocks. Thus, the calculated values of *Le* are likely to be good measures of field-line lengths for spike and pulse events, but only upper limits for ramp events. We have calculated the mean, median, and standard deviations of *Le* for each type of event, independent of the ICME associations, and obtain (Table 2): spikes (mean = 1.61, median = 1.52, standard deviation = 0.34 AU for 47 events); pulses (1.66, 1.63, 0.28 AU for 53 events); and ramps (1.94, 1.90, 0.47 AU for 95 events). The statistically larger ramp values of *Le* are consistent with delayed injections from shocks and also with the inferred longer injection delay times when *Le* = 1.2 AU is assumed (Figure 6(c) of Haggerty & Roelof 2009). We would therefore prefer to limit the ICME *Le* analysis to only the spikes and pulses. However, 14 of the 24 electron events in ICMEs are ramps, so we have included all three event categories in this analysis to optimize the statistics. This should not pose a problem as long as we limit our analysis to comparisons between EPAM electron events inside and outside ICMEs.

Table 3
Differing ICME and Electron-source Active Regions

Electron Event Date	S/C	ICME[a]	ICME Source AR & Latitude	LASCO CME Date & UT	Electron Source AR & Latitude	Source ΔLong	Source ΔLat
1998 Sep 25	EPAM	MC	8340 N20°	Sep 23 0700	8344 S19°	11°	39°
2000 Nov 7	3DP	MC	9213 N02°	Nov 3 1826	9210 S27°	20°	29°
2001 Sep 24	EPAM	1	9631 N08°	Sep 20 1931	9632 S19°	88°	27°
2004 Aug 30	3DP	MC	10664 S10°	Aug 26 1230	10663 N09°	25°	18°
2005 May 16	EPAM	2	10759 N11°	May 13 1712	10763 S15°	37°	26°

Note. [a] MC is true magnetic cloud; 1 and 2 are Richardson & Cane (2010) ICME classes.

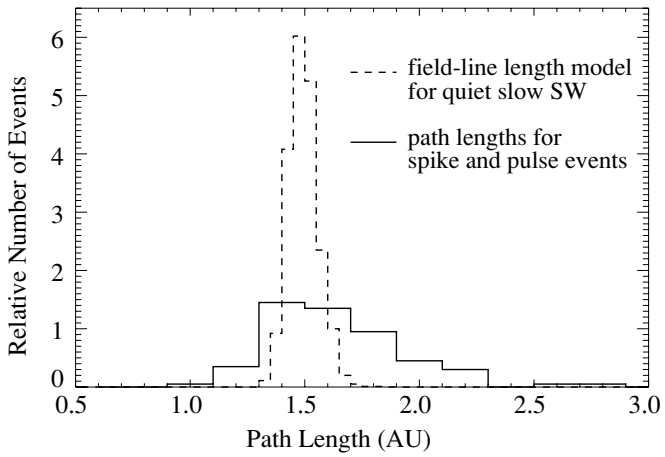

Figure 7. Comparison of the magnetic field-line length distributions of the combined spike and pulse EPAM NR electron events (solid line) and the distribution of model realizations of Ragot (2006) with a single slow solar wind turbulent spectrum and speed of 370 km s^{-1} (dashed line).

The range of *Le* values for the spike and pulse events significantly exceeds the nominal value of ∼1.2 AU for the average quiet spiral field-line length, but those values may serve as good measures of the interplanetary field-line lengths to 1 AU. We can compare the combined spike/pulse *Le* distribution with a distribution calculated for turbulent field-line lengthening with the technique of Ragot (2006). Ragot & Kahler (2008) have presented values of the lengthening factors computed from three-dimensional isotropic turbulent spectra. Figure 7 shows that the spike/pulse event and model mean values of 1.64 and 1.50 AU, respectively, are similar. The event standard deviation of 0.31 AU exceeds the model value of 0.06 AU, but the model realizations presented here were restricted to a single solar wind speed of 370 km s^{-1} and a relatively quiet slow wind turbulent spectrum.

3.4. Comparison of Electron and ICME Solar Sources

As another approach to understanding electron propagation in ICMEs, we compare the solar source regions of the ICMEs with those of the electron events of Table 1 observed within the ICMEs. The LASCO CME sources and their associated flare or eruptive event associations were taken from Richardson & Cane (2010) and Gopalswamy et al. (2009a, 2010). The decametric type III burst times provide good fiducials for the electron events, and we used the LASCO online CME catalog (http://cdaw.gsfc.nasa.gov/CME_list/; Gopalswamy et al. 2009b) and associated solar event-time plots and Solar-Geophysical Data Reports (ftp://ftp.ngdc.noaa.gov/STP/SOLAR_DATA/) to determine the associated flare locations. The purpose is to determine whether the two source regions are roughly co-located, as was the case for the ICME and electron events of 1995 October (Larson et al. 1997; Smith et al. 1997). If an ICME maintains its magnetic connection to the Sun, then we might expect the source of an associated electron event also to lie within the connected region.

Comparing the source ARs identified for the 24 CMEs and electron events inside the ICMEs, we found matching ARs for 13 events, different for 3, and uncertain for 8. We expanded the search to include the 3DP electron events in the eight MCs of Kahler et al. (2011), and there we found three matching, two different, and three uncertain. Thus, around 50% of electron events observed in ICMEs occurred in or near the parent ARs of the ICMEs, and 16% originated in different ARs. The association is uncertain for 34% of the events. The five cases of different ICME/electron-source ARs are listed in Table 3. The first five columns give the dates of the electron events, the observing instruments (3DP/*Wind* or EPAM/*ACE*), the ICME classes, the ICME source AR numbers, and the times of the LASCO associated CMEs. The last three columns of Table 3 give the NR electron-source AR numbers and the longitude and latitude differences of the two source ARs. The 2005 May 16 electron event occurred in a class 2 ICME, but not inside the MC itself. In all five cases, the ICME and electron-source ARs were in opposite hemispheres, and the longitude separations ranged from 11° to 37° in four cases, with a remarkable 88° separation for the 2001 September 24 event.

4. DISCUSSION

4.1. ICME Magnetic Field-line Lengths

The goal of this work is to extend to all ICMEs the earlier analysis of Kahler et al. (2011) using NR solar energetic electron events as probes of field-line lengths in MCs. The path lengths inferred for the first arriving electrons are assumed to be equal to the lengths of the magnetic field lines traced by the electrons from their coronal sources to the *ACE* spacecraft. With a set of 195 beamed EPAM events, we have examined 40 electron events detected either inside ICMEs or within 12 hr of ICME intervals. These ICMEs were divided into three magnetic classes, defined by comparison of their characteristics with the classic MC flux rope (Klein & Burlaga 1982). The 40 inferred *Le* values were compared with those inferred for the ambient solar wind. We found comparable median values of $Le = 1.68$ AU for the former and $Le = 1.70$ AU for the latter. There was no significant difference in *Le* among the three ICME classes, and there was no ordering of *Le* relative to the ICME boundaries, which serve as the best tests of the flux-rope models (Kahler et al. 2011). We were limited to only 10 electron events inside or nearby MCs (Figure 6), but their *Le* values also appeared consistent with those of the electron events outside (Figure 4) and inside (Figure 3) ICMEs. The mean (median) *Le* values

of 1.70 (1.57) AU for the 16 events in class 2 ICMEs of this study are somewhat lower than the 2.27 (2.00) AU *Le* values we calculate for the 30 3DP MC electron events of Table 1 of Kahler et al. (2011). However, the differences are less than a standard deviation (Table 2) and may be due to the selection of beamed EPAM electron events, which may be less scattered than the 3DP MC electron events.

Field-line lengths in flux-rope ICMEs are expected to exceed those in the quiet solar wind, but the primary result here is that we find no evidence for that difference. The limitation on field-line lengths imposes a limit on the number of possible field-line rotations about the flux-rope axis, a basic model parameter. Assuming a flux-rope of axial length X, minor radius R, and a field-line length L in a simple cylindrical flux-rope geometry, we can estimate the number of field-line rotations N from the Sun to 1 AU from

$$X^2 + (R\Phi)^2 = L^2, \quad (1)$$

where Φ is the total rotation angle in radians. Then we get

$$N = \frac{1}{2\pi}\left(\frac{L^2}{X^2} - 1\right)^{1/2}\frac{X}{R}. \quad (2)$$

Taking $X = 1.35$ AU (Kahler et al. 2011), R/X as ~0.05–0.3 (Larson et al. 1997; Leamon et al. 2004; Gulisano et al. 2005), and an upper limit of $L = Le = 2.3$ AU for the ICMEs (Figure 3), we get a range of $N \sim 0.7$–5 rotations and $2N \sim 1.5$–10 rotations for the total number of turns over the full length of a symmetric flux rope. With the mean value of $Le = 1.7$ AU (Figure 3), $2N \sim 0.8$–5 rotations. For a direct comparison with some recent flux-rope models, we use $2\pi N/X = \tau$, the twist, calculated in units of rad AU^{-1}. Thus, $3\,\mathrm{rad\,AU^{-1}} \leqslant \tau \leqslant 24$ rad AU^{-1} for our upper limit of $L = 2.3$ AU. These values are based on a simple cylindrical geometry, so they represent only crude approximations to the MC structures.

Gulisano et al. (2005) have calculated τ_0, the axial twist, for 20 MCs with four different flux-rope models. In three of the models the field-line twist is radius dependent, so we can make a direct comparison of our *Le* values with τ_0 only for the Gold–Hoyle radius-independent model values of their Figure 5, which lie in the range of ~10–30 rad AU^{-1}, in good agreement with our range of ~3–24 rad AU^{-1} for our upper limit of $Le = 2.3$ AU. Since the model twist is distributed mostly in the periphery of the flux rope (Dasso et al. 2006), we can expect peripheral values of τ to be much higher than the range of $5\,\mathrm{rad\,AU^{-1}} \leqslant \tau_0 \leqslant 15$ rad AU^{-1} shown for their other three models. Leamon et al. (2004) have calculated an average value of $\tau = 18$ rad AU^{-1} for 12 MCs using the Lundquist model of Lepping et al. (1990). Those values would exceed our range of $1.9\,\mathrm{rad\,AU^{-1}} \leqslant \tau \leqslant 11.6$ rad AU^{-1} using the mean value of $Le = 1.7$ AU which is derived from all ICMEs, not only the MCs. However, our Figure 5 indicates no significant difference of *Le* among the three ICME classes, so use of τ based on the mean value of *Le* seems appropriate for the comparison.

To summarize, MC model flux-rope calculations indicate significantly longer path lengths than we infer from EPAM electron events. The lack of a significant difference in path lengths among all ICMEs, the MCs separately, and the ambient solar wind does not support the flux-rope models. However, the small number of ICME and MC events included in this study and the lack of a comparison with specific model calculations as carried out in Kahler et al. (2011) do not allow us to rule out the flux-rope models. Our results may provide support for recent MC models in which the observed field rotations are the result of an acquired writhe of the field (Jacobs et al. 2009; Török et al. 2010) rather than twist or in which the axial length over which the twist extends is limited to $\leqslant 1$ AU (Yamamoto et al. 2010).

4.2. Electron Event Profiles and Interplanetary Magnetic Field-line Lengths

Our assumption of electron injections during decametric type III bursts allowed us to test and support the conclusion of Haggerty & Roelof (2009) that their ramp electron events, in which the rapid rises of the intensity–time profiles are followed by plateaus, are due to delayed injections at CME-driven shocks. Injections of the spike and pulse electron events, on the other hand, appear consistent with times of decametric type III bursts. The longer average *Le* of the electron ramp events compared with the combined pulse and spike events (1.94 versus 1.64 AU) supports the contention of Haggerty & Roelof (2009) that the ramp events are due to injection from CME-driven shocks.

The assumed injection times of the spike and pulse events during decametric type III bursts also allowed us to compare the values of *Le* inferred for those events with the distribution of interplanetary field-line lengths calculated with a radially dependent quiet solar wind turbulent spectrum using the method of Ragot (2006). The average field-line lengths are similar in each case (Figure 7). The width of the distribution for the electron events exceeded that of the turbulent model by a factor of ~5, but the narrow width of the latter is due to the use of a single relatively quiet turbulent spectrum and a solar wind speed fixed at 370 km s^{-1}. Assuming a more representative range of solar wind speeds would somewhat broaden the distribution, but the large dynamic range of the observed turbulent spectral amplitudes is the dominant driver that would produce a broader distribution and shift the peak value to larger path lengths, more in agreement with those of the NR electron events.

4.3. Electron-source Regions and Coronal Restructuring

If ICMEs maintain a magnetic connection close to their solar source ARs, we would expect that electrons observed in those ICMEs would have been injected from the same ARs. This is the case for at least half of the ICMEs of this study, but we found five examples (Table 3) in which the injection ARs were different from the ICME source ARs, separated typically by several tens of degrees. This suggests that electrons can access ICMEs from locations well outside the source region of the ICME. One possible scenario is that the electrons were injected from shocks spanning large angular distances in the corona that encounter ICME field lines. If so, we would expect the three EPAM events of Table 3 to be ramps, consistent with a shock origin (Haggerty & Roelof 2009). However, only the 2001 September 24 event was a ramp, while the 1998 September 25 and 2005 May 16 events were spikes. This suggests that shock acceleration is unlikely to explain how electrons associated with an event in one AR are able to access a magnetically closed MC or an ICME originating from a different AR. Comparisons of flare source locations with potential field source surface maps of the solar magnetic field show that electron injections can populate open fields above ARs extending over tens of degrees in longitude (Klein et al. 2008). However, the electrons appear to be restricted to AR field lines (Rust et al. 2008) and so are unlikely to populate field lines in ICMEs from other ARs.

Another possibility is that the ICME magnetic connections to the Sun undergo a dispersal away from the ICME source AR

by interchange reconnections with loops of adjacent regions (Attrill et al. 2008). The solar signature of magnetically opened fields is the coronal dimming, observed best in the EUV and usually characterized by a dark core region and more diffuse spatially extended regions (Attrill et al. 2007). Studies of major flare-CME events have shown dimmings in extensive loop systems that range over more than 100° in longitude and latitude and connect multiple ARs including transequatorial loops (Grechnev et al. 2005; Zhang et al. 2007). Recent observations of coronal dimmings and associated brightenings have shown a CME open-field footprint to extend up to 1 $R_\odot$ for an isolated AR (Attrill et al. 2009).

The original ICME fields can reconnect laterally by a stepping reconnection with loop fields of opposite polarities (Attrill et al. 2007) or by reconnection with overlying loops described by the breakout model (Cohen et al. 2010). Simulations by Gibson & Fan (2008) and Jacobs et al. (2009) show how a writhing erupting flux rope first reconnects with external fields to form new connectivity with one footpoint in the AR bipole and one in the external fields, followed by a further reconnection at a central current sheet that produces a flux rope with both footpoints outside the original AR bipole, which may initially show the darkest dimming. While the numerical simulations have shown good evidence of coronal magnetic reconnection in CMEs (Cohen et al. 2009, 2010), the dimmings recover as loops reform (Attrill et al. 2010), and it is not obvious how the original ICME magnetic connections to the corona are changed. We take our five cases of different ICME-electron-source ARs as additional supporting evidence for significant reconnection of ICME fields with distant coronal fields following the eruption of the source CME. The solar magnetic connections could be transformed further by reconnections observed preferentially in the low-β plasma sheets of ICMEs (Phan et al. 2010).

5. SUMMARY

The estimation of magnetic field-line lengths is important for testing flux-rope models of MCs. The sole observational touchstone for modelers has long been the work of Larson et al. (1997) using the 3DP/*Wind* electron observations in a single MC. We have used the EPAM beamed NR electron events to extend the study of field-line lengths to other ICMEs by assuming that electron injections occur at the times of decametric type III bursts. This is an inversion of the previous technique of assuming a fixed 1.2 AU travel distance to deduce the solar-electron injection times. We find no difference of field-line lengths between electron events in ICMEs and those of the ambient solar wind outside ICMEs. Furthermore, the field-line lengths in MCs show no differences from those of other ICMEs not showing full flux-rope magnetic signatures. The number of field-line rotations over the assumed ICME full length of 2.7 AU is estimated to be 1–10 turns, generally less than that required for most MC flux-rope model fits.

We compared source regions of NR electron events and the ICMEs in which they were detected. In five cases, three from the present study and two from a previous study, the solar NR electron injection regions were well separated spatially from those generating the ICMEs. These results support models of substantial reconnection between erupting CMEs and adjacent or overlying magnetic fields outside the source ARs.

The beamed EPAM NR electron events were classified on the basis of their intensity–time profiles as spike, pulse, and ramp. The inferred path lengths were statistically longer for the ramp events, consistent with a shock source (Haggerty & Roelof 2009) that would delay the solar injection relative to the decametric type III burst. Assuming that the spike and pulse electrons were injected at the decametric type III burst times, we compared their inferred field-line lengths with the distribution of field-line lengths calculated for a turbulent spectrum and found good agreement.

We thank B. Ragot for her model field-line length calculation and plot in Figure 7. We benefited from use of the LASCO CME catalog, which is generated and maintained at the CDAW Data Center by NASA and The Catholic University of America in cooperation with the Naval Research Laboratory. *SOHO* is a project of international cooperation between ESA and NASA. We acknowledge the extensive use of data sets provided at the Web sites of the NASA *Wind* and *ACE* missions.

REFERENCES

Attrill, G. D. R., Engell, A. J., Wills-Davey, M. J., Grigis, P., & Testa, P. 2009, ApJ, 704, 1296
Attrill, G. D. R., Harra, L. K., van Driel-Gesztelyi, L., & Démoulin, P. 2007, ApJ, 656, L101
Attrill, G. D. R., Harra, L. K., van Driel-Gesztelyi, L., & Wills-Davey, M. J. 2010, Sol. Phys., 264, 119
Attrill, G. D. R., van Driel-Gesztelyi, L., Démoulin, P., Zhukov, A. N., Steed, K., Harra, L. K., Mandrini, C. H., & Linker, J. 2008, Sol. Phys., 252, 349
Bougeret, J.-L., et al. 1995, Space Sci. Rev., 71, 231
Broderick, A. E., & Blandford, R. D. 2010, ApJ, 718, 1085
Byrne, J. P., Maloney, S. A., McAteer, J., Refojo, J. M., & Gallagher, T. 2010, Nat. Commun., 74, 1
Cane, H. V. 2003, ApJ, 598, 1403
Cane, H. V., & Richardson, I. G. 2003, J. Geophys. Res., 108, 1156
Chen, J., & Kunkel, V. 2010, ApJ, 717, 1105
Cohen, O., Attrill, G. D. R., Manchester, W. B., & Wills-Davey, M. J. 2009, ApJ, 705, 587
Cohen, O., Attrill, G. D. R., Schwadron, N. A., Crooker, N. U., Owens, M. J., Downs, C., & Gombosi, T. I. 2010, J. Geophys. Res., 115, A10104
Crooker, N. U., Kahler, S. W., Gosling, J. T., & Lepping, R. P. 2008, J. Geophys. Res., 113, A12107
Crooker, N. U., & Pagel, C. 2008, J. Geophys. Res., 113, A02106
Dasso, S., Mandrini, C. H., Démoulin, P., & Luoni, M. L. 2006, A&A, 455, 349
Davis, C. J., Davies, J. A., Lockwood, M., Rouillard, A. P., Eyles, C. J., & Harrison, R. A. 2009, Geophys. Res. Lett., 36, L08102
Gibson, S. E., & Fan, Y. 2008, J. Geophys. Res., 113, A09103
Gold, R. E., et al. 1998, Space Sci. Rev., 86, 541
Gopalswamy, N., Akiyama, S., Yashiro, S., Michalek, G., & Lepping, R. P. 2009a, J. Atmos. Sol.-Terr. Phys., 71, 1005
Gopalswamy, N., Xie, H., Mäkelä, P., Akiyama, S., Yashiro, S., Kaiser, M. L., Howard, R. A., & Bougeret, J.-L. 2010, ApJ, 710, 1111
Gopalswamy, N., Yashiro, S., Michalek, G., Vourlidas, A., Freeland, S., & Howard, R. 2009b, Earth Moon Planets, 104, 295
Grechnev, V. V., et al. 2005, J. Geophys. Res., 110, A09S07
Gulisano, A. M., Dasso, S., Mandrini, C. H., & Démoulin, P. 2005, J. Atmos. Terr. Phys., 67, 1761
Haggerty, D. K., & Roelof, E. C. 2002, ApJ, 579, 841
Haggerty, D. K., & Roelof, E. C. 2006a, Adv. Space Res., 38, 990
Haggerty, D. K., & Roelof, E. C. 2006b, Adv. Space Res., 38, 1001
Haggerty, D. K., & Roelof, E. C. 2009, in AIP Conf. Proc. 1183, Shock Waves in Space and Astrophysical Environments, ed. X. Ao, R. H. Burrows, & G. P. Zank (Melville, NY: AIP), 3
Haggerty, D. K., Roelof, E. C., & Simnett, G. M. 2003, Adv. Space Res., 32, 2673
Jacobs, C., Roussev, I. I., Lugaz, N., & Poedts, S. 2009, ApJ, 695, L171
Jensen, E. A., & Russell, C. T. 2008, Geophys. Res. Lett., 35, L02103
Jones, G. H., Rees, A., Balogh, A., & Forsyth, R. J. 2002, Geophys. Res. Lett., 29, 11
Kahler, S. W., Aurass, H., Mann, G., & Klassen, A. 2007, ApJ, 656, 567
Kahler, S. W., Krucker, S., & Szabo, A. 2011, J. Geophys. Res., 116, A01104
Kilpua, E. K. J., et al. 2009, Sol. Phys., 254, 325
Klein, K.-L., Krucker, S., Lointier, G., & Kerdraon, A. 2008, A&A, 486, 58
Klein, K.-L., Krucker, S., Trottet, G., & Hoang, S. 2005, A&A, 431, 1047
Klein, L. W., & Burlaga, L. F. 1982, J. Geophys. Res., 87, 613
Krall, J. 2007, ApJ, 657, 559

Kunkel, V., & Chen, J. 2010, ApJ, 715, L80
Larson, D. E., et al. 1997, Geophys. Res. Lett., 24, 1911
Leamon, R. J., Canfield, R. C., Jones, S. L., Lambkin, K., Lundberg, B. J., & Pevtsov, A. A. 2004, J. Geophys. Res., 109, A05106
Lepping, R. P., Burlaga, L. F., & Jones, J. A. 1990, J. Geophys. Res., 95, 11957
Lepping, R. P., & Wu, C.-C. 2010, Ann. Geophys., 28, 1539
Liu, Y., Luhmann, J. G., Huttunen, K. E. J., Lin, R. P., Bale, S. D., Russell, C. T., & Galvin, A. B. 2008a, ApJ, 677, L133
Liu, Y., Manchester, W. B., IV, Kasper, J. C., Richardson, J. D., & Belcher, J. W. 2007, ApJ, 665, 1439
Liu, Y., et al. 2008b, ApJ, 689, 563
Lynch, B. J., Li, Y., Thernisien, A. F. R., Robbrecht, E., Fisher, G. H., Luhmann, J. G., & Vourlidas, A. 2010, J. Geophys. Res., 115, A07106
Maia, D. J. F., & Pick, M. 2004, ApJ, 609, 1082
McComas, D. J., Gosling, J. T., Bame, S. J., Smith, E. J., & Cane, H. V. 1989, J. Geophys. Res., 94, 1465
Moldwin, M. B., Siscoe, G. L., & Schrijver, C. A. 2009, in Heliophysics: Plasma Physics of the Local Cosmos, ed. C. J. Schrijver & G. L. Siscoe (Cambridge: Cambridge Univ. Press), 139
Möstl, C., Farrugia, C. J., Temmer, M., Miklenic, C., Veronig, A. M., Galvin, A. B., Leitner, M., & Biernat, H. K. 2009b, ApJ, 705, L180
Möstl, C., et al. 2009a, J. Geophys. Res., 114, A04102
Nakagawa, T., & Matsuoka, A. 2010, J. Geophys. Res., 115, A10113
Nindos, A., Aurass, H., Klein, K.-L., & Trottet, G. 2008, Sol. Phys., 253, 3
Odstrcil, D., & Pizzo, V. J. 1999, J. Geophys. Res., 104, 28225
Owens, M., & Cargill, P. 2004, Ann. Geophys., 22, 4397
Phan, T. D., et al. 2010, ApJ, 719, L199
Qiu, J., Hu, Q., Howard, T. A., & Yurchyshyn, V. B. 2007, ApJ, 659, 758
Ragot, B. R. 2006, ApJ, 653, 1493
Ragot, B. R., & Kahler, S. W. 2008, in Proc. 30th Int. Cosmic Ray Conf., Mérida, Yucatán, Mexico, Vol. 1, ed. R. Caballero, J. C. D'Olivo, G. Medina-Tanco, L. Nellen, F. A. Sánchez, & J. F. Valdés-Galicia (Mexico City: Universidad Nacional Autónoma de México), 147
Richardson, I. G., & Cane, H. V. 2010, Sol. Phys., 264, 189
Rust, D. M., David, M., Haggerty, D. K., Georgoulis, M. K., Sheeley, N. R., Wang, Y.-M., De Rosa, M. L., & Schrijver, C. J. 2008, ApJ, 687, 635
Simnett, G. M. 2007, A&A, 472, 309
Simnett, G. M., Roelof, E. C., & Haggerty, D. K. 2002, ApJ, 579, 854
Smith, Z., Watari, S., Dryer, M., Manoharan, P. K., & McIntosh, P. S. 1997, Sol. Phys., 171, 177
Temmer, M., Veronig, A. M., Kontar, E. P., Krucker, S., & Vršnak, B. 2010, ApJ, 712, 1410
Török, T., Berger, M. A., & Kliem, B. 2010, A&A, 516, A49
Wang, L., Lin, R. P., Krucker, S., & Gosling, J. T. 2006, Geophys. Res. Lett., 33, L03106
Wang, Y.-M., & Sheeley, N. R., Jr. 2006, ApJ, 650, 1172
Wood, B. E., & Howard, R. A. 2009, ApJ, 702, 901
Wood, B. E., Howard, R. A., & Socker, D. G. 2010, ApJ, 715, 1524
Yamamoto, T. T., Kataoka, R., & Inoue, S. 2010, ApJ, 710, 456
Zhang, Y., Wang, J., Attrill, G. D. R., Harra, L. K., Yang, Z., & He, X. 2007, Sol. Phys., 241, 329
Zurbuchen, T. H., & Richardson, I. G. 2006, Space Sci. Rev., 123, 31

DISTRIBUTION LIST

DTIC/OCP
8725 John J. Kingman Rd, Suite 0944
Ft Belvoir, VA 22060-6218 1 cy

AFRL/RVIL
Kirtland AFB, NM 87117-5776 2 cys

Official Record Copy
AFRL/RVBXS/Donald Norquist 1 cy